Spectroscopic Study of Substrate Binding to the Carbonmonoxy Form of Dehaloperoxidase from *Amphitrite ornata*

Karin Nienhaus,[†] Pengchi Deng,[†] Jennifer Belyea,[‡] Stefan Franzen,*[,‡] and G. Ulrich Nienhaus*[,†,§]

Department of Biophysics, University of Ulm, Albert-Einstein-Allee 11, D-89081 Ulm, Germany, Department of Chemistry, North Carolina State University, Raleigh, North Carolina 27695, and Department of Physics, University of Illinois at Urbana−Champaign, 1110 West Green Street, Urbana, Illinois 61801

Received: January 15, 2006; In Final Form: April 30, 2006

Dehaloperoxidase (DHP) is a globular heme enzyme found in the marine worm *Amphitrite ornata* that can catalyze the dehalogenation of halophenols to the corresponding quinones by using hydrogen peroxide as a cosubstrate. Its three-dimensional fold is surprisingly similar to that of the oxygen storage protein myoglobin (Mb). A key structural feature common to both DHP and Mb is the existence of multiple conformations of the distal histidine. In DHP, the conformational flexibility may be involved in promotion of substrate and cosubstrate entry and exit. Here we have explored the dynamics of substrate binding in DHP using Fourier transform infrared spectroscopy and flash photolysis. A number of discrete conformations at the active site were identified from the appearance of multiple CO absorbance bands in the infrared region of the spectrum. Upon photolysis at cryogenic temperatures, the CO molecules are trapped at docking sites within the protein matrix, as inferred from the appearance of several photoproduct bands characteristic of each site. Substrate binding stabilizes the protein by ∼20 kJ/mol. The low yield of substrate-bound DHP at ambient temperature points toward a steric inhibition of substrate binding by carbon monoxide.

Introduction

A novel globin known as dehaloperoxidase (DHP), first isolated from the marine worm *Amphitrite ornata*, is a peroxidase that has striking structural similarities with myoglobins and hemoglobins.[1] The polypeptide chains of DHP and myoglobin (Mb) are arranged in eight α-helices surrounding a heme prosthetic group (Figure 1a), the central iron atom of which binds diatomic ligands such as dioxygen (O_2), carbon monoxide (CO), and nitric oxide (NO).[2] Although Mb has been viewed as a simple oxygen storage protein for many years, a novel physiological role as an NO scavenger has been proposed recently.[3] Myoglobin is also known to catalyze various oxidation reactions, though not very efficiently.[4−8] Dehaloperoxidase may also function as an oxygen storage protein, but more intriguing is the fact that DHP is capable of catalytic degradation of halophenols secreted by marine worms such as *Thelepus crispus* and *Notomastus lobatus* that cohabit mudflats with *Amphitrite ornata*.[9−12] The enzyme requires hydrogen peroxide (H_2O_2) or other peroxides to catalyze the dehalogenation of trihalogenated phenols into dihalogenated quinones. However, it is not selective for trihalogenated phenols and will also oxidize mono- and dihalophenols. Franzen and co-workers have recently shown that substrate binding must precede H_2O_2 binding to allow for an efficient peroxidase function.[13]

Heme peroxidases are among the most extensively studied groups of enzymes. Horseradish peroxidase (HRP) catalyzes the H_2O_2-dependent oxidation of a variety of aromatic electron donor molecules such as benzhydroxamic acid.[14] Lignin peroxidase (LIP) plays a central role in the biodegradation of the plant cell wall constituent lignin.[15] In peroxidase function, the heme iron is initially oxidized by H_2O_2. The resulting species, compound I, is reduced in a two-step process via intermediate compound II to restore the resting state. The substrate is oxidized in this process, either in two individual steps (2 equiv of substrate per cycle) or in a two-step oxidation reaction (1 equiv per cycle). The basic reaction mechanism was proposed by Poulos and Kraut in 1980[16] and has since then been studied in great detail.[14,15,17,18] Strong hydrogen bonding interactions between the proximal histidine and the neighboring residues facilitate H_2O_2 cleavage. This so-called push effect is markedly enhanced in chloroperoxidase and P450, where the proximal histidine is replaced by a cysteine.[19] The distal histidine and an arginine residue exert an additional pull from the distal side of the heme in most histidine-ligated heme-containing enzymes. Remarkably, DHP lacks both the strong hydrogen bonding network on the proximal side and the arginine residue on the distal side. However, the distal pocket contains a histidine (His55), which is positioned 5.4 Å from the heme iron and thus ∼1.5 Å further away than the corresponding histidine in Mb (His64). This distance is similar to the one found in peroxidases.[20] The His55 imidazole may adopt both an open and a closed conformation, as is observed in the X-ray structure of ferric DHP (Figure 1b). When buried in the distal pocket (i.e., in the substrate-free form), it is rotated by ∼90° about an axis perpendicular to the imidazole ring plane relative to the His64 imidazole of Mb. With a substrate analog (4−iodophenol) inside the distal heme pocket, the distal His55 side chain is rotated toward the solvent into a position at least 9 Å from the heme iron.[20] Therefore, assuming substrate binding initiates the enzymatic reaction, it seems unlikely that the side chain acts as

* Authors to whom correspondence should be addressed. E-mail: Stefan.Franzen@ncsu.edu (S.F.); uli@uiuc.edu (G.U.N.).
[†] University of Ulm.
[‡] North Carolina State University.
[§] University of Illinois at Urbana−Champaign.

10.1021/jp060278z CCC: $33.50
Published on Web 06/09/2006

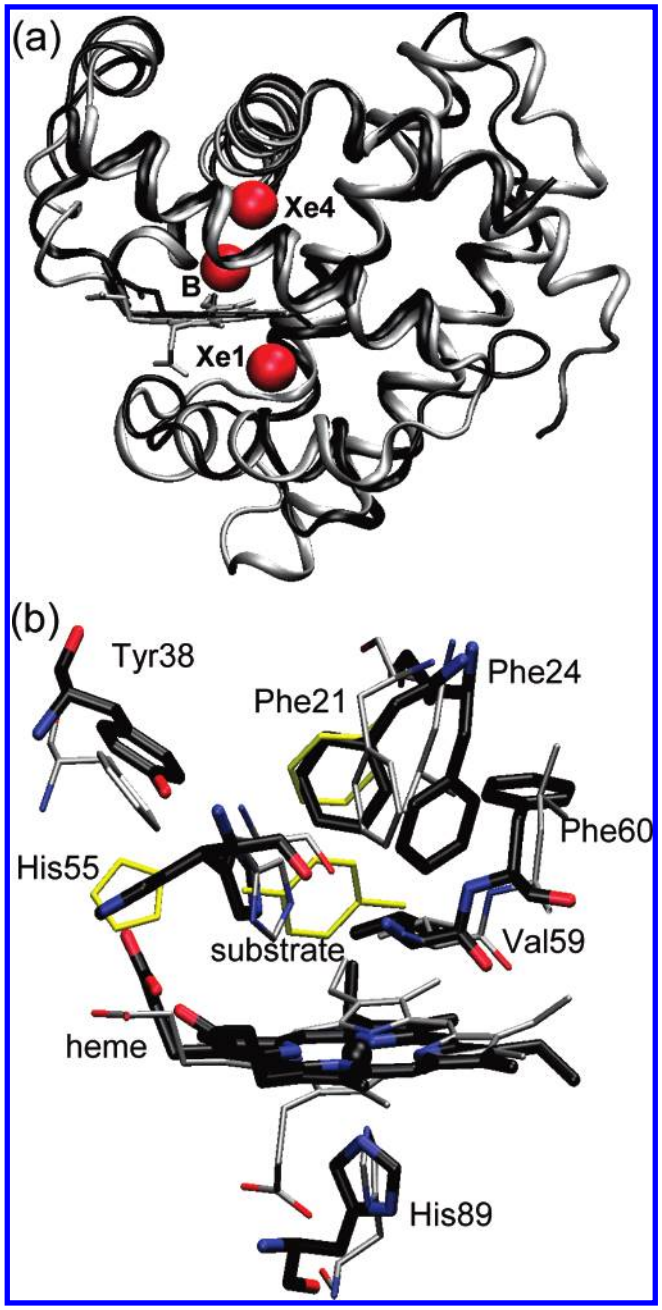

Figure 1. (a) Ribbon representations of the overall structures of DHP (black, PDB code 1EWA) and Mb (gray, PDB code 1JDO). The transient ligand docking sites B, Xe4, and Xe1 in Mb are included as red spheres. (b) Overlay of the active-site structures of ferric DHP (black, 1EWA and 1EW6) and Mb mutant Leu29Phe (gray, 1JDO). The DHP substrate 4-iodophenol is included in yellow.

a catalyst upon H_2O_2 binding, as proposed by the Poulos−Kraut mechanism.[16] These considerations add to the interest in determining the mechanistic role of the active-site amino acids and especially of the distal His55 in DHP.

Many peroxidases are involved in the degradation of pathogenic compounds. In the enzymatic action of HRP and other peroxidases, the substrate remains at the edge of the heme plane and does not enter the protein interior.[17,18,21] By contrast, DHP appears to accommodate the substrate in a well-defined substrate-binding pocket. To shed light on the interaction between the protein and the phenolic substrate, a sensitive local gauge is required that reports substrate binding. Here we have utilized the CO molecule to probe the active-site structure. Its stretching vibration absorbs strongly in the infrared at ∼5 μm, and its absorption frequency is sensitive to the interaction between the CO dipole and the local electric field (Stark effect).[22,23] Each discrete active-site conformation gives rise to a specific absorbance band of the heme-bound CO in the region between 1900 and 2000 cm^{-1}, as is observed for MbCO, where different orientations of the distal histidine are responsible for the three so-called A substate bands, A_0, A_1, and A_3.[24,25] From the multiple conformations of His55 in the X-ray structure,[20] we anticipated that DHP likewise shows multiple stretching bands.

In heme proteins, the covalent bond between the iron and CO can be ruptured by visible light. At cryogenic temperatures, photodissociated CO ligands remain trapped within the protein matrix. If structurally well-defined docking sites exist, then narrow photoproduct bands, with stretching frequencies characteristic of each site, can be observed in the region between 2100 and 2160 cm^{-1}.[26,27] In fact, two photoproduct bands that arise from opposite orientations of the CO are frequently associated with a single docking site.[28−30] In MbCO, photodissociated CO molecules have been observed at the primary docking site B and at the secondary sites C (Xe4) and D (Xe1), with the latter two corresponding to two out of four hydrophobic cavities present in the protein matrix.[28,31−37]

To utilize the superb properties of CO as a local structural probe, we have prepared the CO-ligated ferrous form of DHP (DHPCO) in the absence and presence of different substrates. We have studied the structural heterogeneity of this novel globin enzyme at the molecular level by using Fourier transform infrared (FTIR) and time-resolved visible spectroscopy. We have also investigated the DHP mutant Tyr38Phe, which has a tyrosine at position 38 in the CD loop (CD4) replaced by a phenylalanine. The corresponding amino acid Phe46 in Mb has been shown to orient the distal His64 for hydrogen bonding to heme-bound ligands.[38] From removing the interaction between the Tyr38 hydroxyl and the His64 imidazole side chain, we anticipated a significant effect on the structural heterogeneity at the active site. This spectroscopic characterization is a first step toward understanding DHP's physiological role as a peroxidase.

Materials and Methods

Sample Preparation. The cloning of 6×His-tagged DHP into the pET16b expression plasmid has been described previously.[13] Except for the additional tag, this recombinant protein has the same primary sequence as the native protein. We will refer to it as the 6×His-tagged protein throughout the paper. The preparation of the Tyr38Phe mutant has been described elsewhere.[39] Infrared samples were prepared by dissolving freeze-dried DHP in glycerol/0.5 M potassium phosphate buffer (50/50 by volume) at a final concentration of 10 mM. We have confirmed that lyophilized, redissolved protein samples have the same enzyme activity as freshly prepared ones (data not shown). Excess imidazole, 2,4,6-tribromophenol (TBP) or 2,4,6-trifluorophenol (TFP) was added for substrate-bound samples. Although the native substrate is TBP, TFP was used in some experiments because of its greater solubility. The sample solution was stirred under a CO atmosphere for 1 h and reduced by adding a 2-fold molar excess of an anaerobically prepared sodium dithionite solution. It was centrifuged for 15 min at 5000*g* (Eppendorf centrifuge) to remove any undissolved material. For low-temperature flash photolysis experiments, dilute samples with a protein concentration of ∼10 μM were prepared in glycerol/0.4 M potassium phosphate buffer (75/25 by volume).

UV−Visible Spectroscopy. Spectra of ∼10 μM ferric samples in 0.1 M buffer (pH < 5, sodium phosphate/citrate,

pH 5−8.5, sodium phosphate, pH > 8.5, sodium carbonate) were recorded with a Cary 1 E spectrometer (Varian, Darmstadt, Germany) at a resolution of 1 nm.

Fourier Transform Infrared Cryospectroscopy and Photolysis Setup. A few microliters of the sample solution were placed between two CaF_2 windows separated by a 75 μM Mylar spacer and loaded into an oxygen-free copper block. The sample holder was mounted on the coldfinger of a closed-cycle helium refrigerator (model SRDK-205AW, Sumitomo, Tokyo, Japan). The sample temperature was measured with a silicon temperature sensor diode and regulated by a digital temperature controller (model 330, Lake Shore Cryotronics, Westerville, OH). The sample was photolyzed with a continuous wave, frequency-doubled Nd:YAG laser (model Forte 530-300, Laser Quantum, Manchester, U. K.), emitting 300 mW output power at 532 nm. The laser beam was split and focused with lenses on the sample from both sides. Fourier transform infrared transmission spectra between 1800 and 2400 cm^{-1} at a resolution of 2 cm^{-1} were obtained with a Bruker IFS 66v/S instrument (Bruker, Karlsruhe, Germany).

Temperature Derivative Spectroscopy. Temperature derivative spectroscopy (TDS) is an experimental protocol designed to study thermally activated rate processes.[40−43] In the first step, a nonequilibrium intermediate state is created by photolysis. Subsequently, the relaxation of the sample back to equilibrium is recorded while the temperature is ramped up linearly in time. One FTIR transmission spectrum is acquired every kelvin. Absorption difference spectra are calculated from consecutive transmission spectra. These data show the changes within 1 K arising not only from recombination but also from intrinsic peak shifts and absorbance changes due to ligand dynamics.[44,45] Fourier transform infrared temperature derivative spectroscopy data are presented as contour plots of the absorbance changes on a surface spanned by temperature and wavenumber. Solid (dotted) lines indicate an absorbance increase (decrease); contours are spaced logarithmically.

Flash Photolysis. The sample was loaded in a 10 × 10 × 2.5 mm^3 poly(methyl methacrylate) cuvette, mounted in a home-built copper sample holder and attached to the coldfinger of a closed-cycle helium cryostat (model 22, CTI Cryogenics, Mansfield, MA), equipped with a Lake Shore Cryotronics (Westerville, OH) model 330 digital temperature controller. Samples were photolyzed by a saturating 6 ns (full width at half-maximum) pulse from a frequency-doubled, Q-switched, Nd:YAG laser (model Surelite II, Continuum, Santa Clara, CA). Light from a tungsten source (model A 1010, PTI, Brunswick, NJ) passed through a monochromator set at 436 nm was used to monitor the photolysis-induced optical absorbance changes. Intensities were measured with a photomultiplier tube (model R5600U, Hamamatsu Corp., Middlesex, NJ) and recorded with a digital storage oscilloscope from 10 ns to 50 μs (model TDS 520, Tektronix, Wilsonville, OR) and a home-built logarithmic time-base digitizer (Wondertoy II) from 2 μs to 100 s.

Results

UV−Visible Spectra of DHP. UV−visible absorption spectroscopy is a valuable tool to monitor the oxidation and ligation state at the heme iron. The spectra of ferric 6×His-tagged DHP are plotted in Figure 2a in the pH range from 5 to 10. At low pH, a water molecule is coordinated to the high-spin ferric heme iron, as can be inferred from the bands at 503, 539, and 636 nm that are typical of an aquomet species. The water molecule is not stabilized by an additional hydrogen bonding interaction to an amino acid side chain, as indicated by the high wavelength

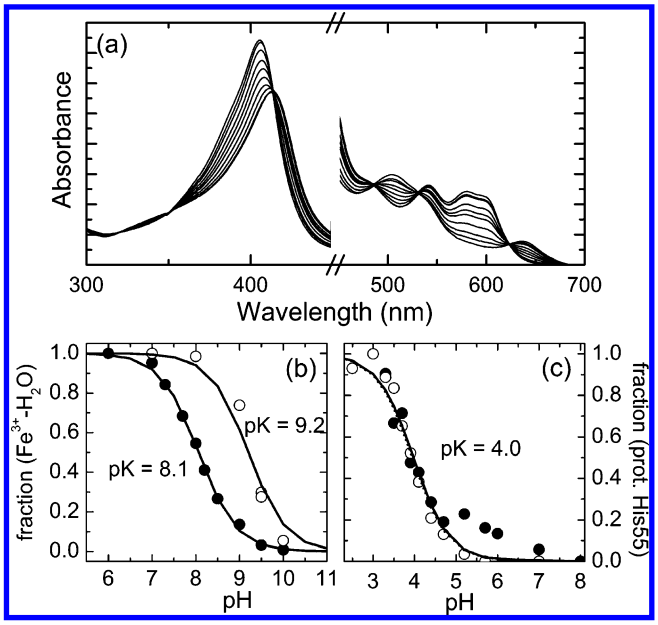

Figure 2. (a) UV−visible spectra of ferric DHP between pH 5 and 10. (b) Scaled absorbance differences at 404 nm as a function of pH. Closed symbols, 6×His-tagged DHP; open symbols, Tyr38Phe; lines, fit to the data with the Henderson−Hasselbalch equation. (c) pH-dependent spectral shifts of the Soret band of DHPCO (open symbols) and Tyr38PheCO (closed symbols), scaled between 0 and 1. Lines represent fits with eq 1.

of the charge-transfer band at 636 nm.[46] As the pH is increased, these bands disappear, and new bands emerge at 540, 579, and 598 nm. Concomitantly, the Soret band shifts from 405 to 410 nm. The equivalent changes in the spectra of mutant Tyr38Phe occur at higher pH values. The rescaled absorbance changes at 404 nm are given in Figure 2b as a function of pH. They follow the Henderson−Hasselbalch relation, which gives the fractional populations of the protonated (acid) and deprotonated (base) species, here denoted by c_+ and c_0, as a function of pH

$$c_+(\mathrm{pH}) = 1 - c_0(\mathrm{pH}) = \frac{1}{1 + 10^{\mathrm{pH}-\mathrm{p}K_a}} \qquad (1)$$

The transition in Figure 2 represents the acid/alkaline transition:[2] The water molecule coordinated to the heme iron at low pH is replaced by the OH^- anion with a pK_a of 8.1 ± 0.1. A typical low-spin alkaline species is characterized by α- and β-bands at ∼540 and 580 nm.[2] The additional band at ∼600 nm indicates that the heme iron exists in a mixture of high- and low-spin states in metDHP−OH at room temperature. The pK_a value of the mutant sample is shifted to 9.2 ± 0.1.

Addition of imidazole leads to a spectrum typical of a bis-histidine-ligated, hexacoordinate ferric heme iron (Supporting Information). This spectral change verifies that imidazole enters the distal pocket of DHP and coordinates to the ferric heme iron as observed in Mb.[2] Upon reduction of the iron, the Soret band of the ferrous deoxy species peaks at 431 nm, with a smaller band due to the α and β transitions at 555 nm. This spectrum is typical of a pentacoordinate ferrous heme iron; it is observed in both the presence and the absence of imidazole. At pH > 9, the deoxy Soret shifts to lower wavelengths (pH 10, 430 nm; pH 11, 429 nm). In contrast, ferrous, CO-ligated 6×His-tagged DHP and Tyr38Phe both have Soret bands at ∼422 nm that shift to the blue with increasing pH. A fit of the scaled wavelength changes with eq 1 identifies a titrating group with a pK_a of 4.0 ± 0.1 (Figure 2c).

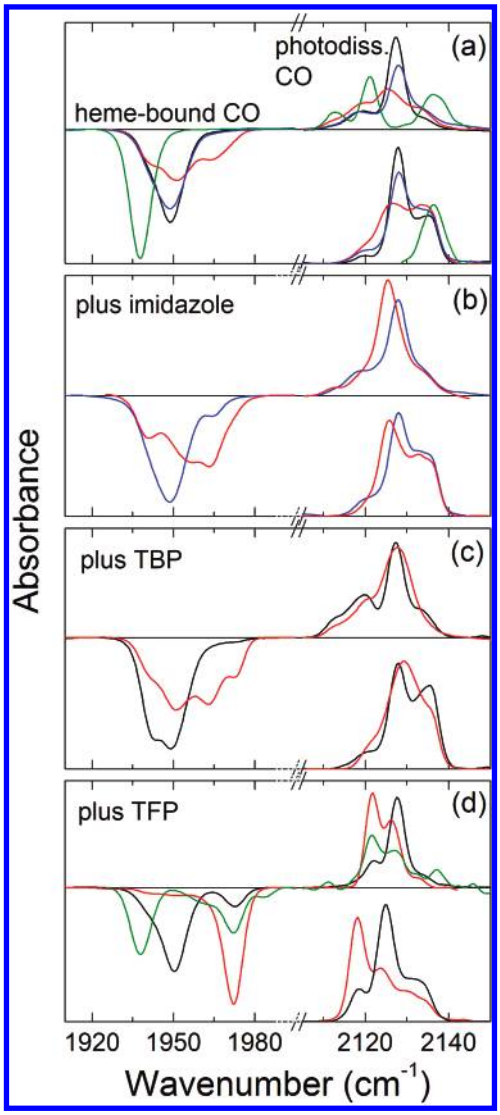

Figure 3. Photolysis difference spectra of CO-ligated DHP, calculated from transmission spectra taken before and after photolysis. Left: Absorbance changes in the bands of heme-bound CO after 1 s of illumination at 3 K. Top right: Absorbance changes in the bands of photolyzed CO after 1 s of illumination at 3 K. Bottom right: Absorbance changes in the bands of photolyzed CO after slow cooling from 160 to 3 K under constant illumination. Black lines, 6×His-tagged DHP, pH 7; red lines, 6×His-tagged DHP, pH 5.5; blue lines, 6×His-tagged DHP, pH 10; green lines, Tyr38Phe, pH 7.5; (a) without substrate, (b) with imidazole, (c) with TBP, (d) with TFP. All spectra have been normalized to equal areas for better comparison.

Fourier Transform Infrared Absorbance Difference Spectra at 3 K. To obtain insight into active-site heterogeneity, absorbance difference spectra of the CO-ligated species were calculated from transmission spectra, I, collected before and after illumination for 1 s at 3 K according to $\Delta A = \log(I_{dark}/I_{light})$. They indicate light-induced absorbance changes in the sample. The spectra of heme-bound and photolyzed CO are shown in Figure 3, normalized to equal areas of 1 and 0.5 OD cm^{-1}, respectively (Figure 3). The A substate bands have a negative sign; they represent CO ligands that have been photodissociated from the heme iron. The photolyzed CO ligands become trapped in internal docking sites where they give rise to new bands with a positive absorbance difference that are about a factor of 20 less intense than the A substate bands. The peak frequencies and relative populations of the bands are compiled in Table 1. The parameters were obtained by nonlinear least-squares fitting of the absorbance difference spectra with sums of Gaussian-shaped lines.

At 3 K, all 6×His-tagged DHP samples show several absorbance bands of heme-bound CO, indicating multiple conformations at the active site. In a substrate-free sample at pH 7, the dominant A band is at 1949 cm^{-1} (Table 1). Minor peaks are located at 1940 and 1960 cm^{-1} (Figure 3a). At pH 5.5, an additional band appears at 1965 cm^{-1} that is more pronounced in the presence of imidazole (Figure 3b). Addition of TBP and especially TFP produces a high-frequency band at 1972 cm^{-1} (Figures 3c and 3d), which is more intense at low pH and even the dominant band in the DHPCO−TFP sample at low pH. Mutant Tyr38Phe (pH 7.5) has only a single A band at 1938 cm^{-1} (Figure 3a, Table 1), and addition of TFP leads to several high-frequency bands; the most prominent one resides at 1972 cm^{-1} (Figure 3d).

In the absence of substrate, the 6×His-tagged DHPCO photoproduct bands are at 2119, 2127 (largest population), and 2133 cm^{-1} at pH 7 after illumination for 1 s. The small band at 2113 cm^{-1} is more pronounced at low pH (Figures 3a−d, top right; Table 1). At pH 5.5, the dominant band sits at 2126 cm^{-1}, whereas it is shifted to 2128 cm^{-1} at pH 10. The positions of the minor bands are not pH-dependent. Likewise, addition of imidazole and TBP does not significantly influence the stretching frequencies of photolyzed CO. With TFP, however, we observe a new photoproduct band at 2122 cm^{-1}; the one at 2118 cm^{-1} is missing. In mutant Tyr38Phe, the photoproduct band at 2127 cm^{-1} is absent; instead, we observe a rather strong peak at 2137 cm^{-1} and additional bands at 2113 and 2121 cm^{-1}. Upon addition of TFP, a new band arises at 2128 cm^{-1} (Table 1).

Extended illumination, especially at higher temperatures, enables ligands to sample more remote secondary docking sites, with higher enthalpy barriers against recombination.[41] Hence, absorbance difference spectra were determined for all samples after photolysis during slow cooling from 160 to 3 K. We present only the 3 K photoproduct spectra in Figure 3 (bottom right) because the bound-state spectra are identical to those obtained after 1 s of illumination. All 6×His-tagged DHPCO spectra exhibit bands at 2120, 2127, 2132, and 2136 cm^{-1} (Table 1). The photoproduct spectrum of mutant Tyr38Phe, however, displays only a single band at 2137 cm^{-1}. With substrate, multiple photoproduct sites are occupied, as inferred from the bands at 2122, 2128, 2133, and 2137 cm^{-1}.

Ligand Recombination after Brief Illumination. Immediately after 1 s of illumination at 3 K, a TDS experiment was started. The temperature ramp ensures that rebinding occurs sequentially with respect to the activation enthalpy barrier that has to be overcome for rebinding to the heme iron.[40] In the following, we will denote the bands of heme-bound (photolyzed) CO using the letter A (B), indicating the peak wavenumber by the subscript.

The absorbance changes of several 6×His-tagged DHP samples are displayed in the TDS maps in Figure 4. At pH 5.5, we observe rebinding from a single photoproduct intermediate for each A substate (Figure 4a) up to temperatures of 100 K. Maximal recombination in A_{1940} and A_{1950} occurs between 30 and 40 K. In the A_{1972} conformation, CO ligands return at ∼10 K in the presence of TBP (not shown) and at ∼35 K if TFP is added (Figure 4e). In the latter sample, a minor fraction also rebinds at ∼10 K. At pH 7, the contours still extend out to ∼100 K (Figure 4c). Recombination in A_{1940} and A_{1950} peaks between 50 and 60 K and thus at higher temperatures as in the pH 5.5 sample. With TBP added to 6×His-tagged DHPCO, no

TABLE 1: Infrared Stretching Frequencies of Heme-Bound and Photolyzed CO in DHP[a]

sample	ν_{CO} (cm^{-1}) (heme-bound CO)				ν_{CO} (cm^{-1}) (photolyzed CO (1 s of illumination))				ν_{CO} (cm^{-1}) (photolyzed CO (slow cool))			
DHP, No Substrate												
pH 7	1940 (15)	1949 (80)	1960 (5)			2119 (24)	2127 (62)	2133 (14)	2120 (5)	2127 (62)	2132 (8)	2136 (25)
pH 5.5	1941 (22)	1951 (46)	1965 (32)		2113 (8)	2119 (23)	2126 (43)	2133 (26)	2120 (10)	2126 (37)	2132 (38)	2136 (15)
pH 10.0	1943 (34)	1959 (61)	1962 (6)			2119 (28)	2128 (50)	2133 (22)	2122 (14)	2128 (44)	2132 (22)	2136 (20)
DHP Plus Imidazole												
pH 5.4					2114 (6)	2119 (9)	2126 (65)	2133 (20)	2120 (4)	2126 (46)	2132 (40)	2136 (9)
pH 10.0	1942 (32)	1950 (58)	1965 (10)			2119 (16)	2128 (53)	2134 (19)	2121 (11)	2128 (49)	2133 (25)	2136 (15)
						2123 (4)						
DHP Plus TBP												
pH 7	1941 (37)	1950 (53)	1959 (8)	1972 (2)	2112 (7)	2119 (33)	2127 (40)	2133 (20)	2120 (11)	2128 (45)	2132 (11)	2136 (33)
pH 5.5	1941 (14)	1951 (40)	1963 (35)	1973 (11)	2114 (8)	2120 (17)	2128 (69)	2135 (6)	2122 (12)	2127 (41)	2132 (32)	2136 (15)
DHP Plus TFP												
pH 7.4	1941 (18)	1951 (65)	1962 (3)	1973 (13)		2122 (26)	2128 (56)	2132 (18)	2122 (15)	2128 (49)	2132 (23)	2136 (13)
pH 5.5	1942 (3)	1952 (6)	1963 (12)	1972 (79)		2122 (47)	2126 (47)	2133 (6)	2122 (46)	2127 (27)	2132 (18)	2136 (9)
Tyr38Phe, pH 7.5												
	1938 (100)				2113 (16)	2121 (40)		2137 (44)				2137 (100)
Tyr38Phe Plus TFP, pH 7.5												
	1938 (49)		1961 (15)	1972 (31)		2121 (27)	2127 (45)	2133 (3)	2122 (32)	2128 (35)	2133 (16)	2137 (17)
				1984 (5)				2137 (15)				

[a] Band positions were determined at 3 K, with an estimated experimental error of ± 1 cm^{-1}. Fractions of the total population are given in brackets (in percent).

temperature shift was observed for rebinding in A_{1972} (data not shown). In the presence of TFP, however, the fraction of molecules recombining at ~10 K is markedly suppressed (Figure 4g). The TDS maps of 6×His-tagged DHPCO at pH 10 are identical to the ones at pH 7. Addition of imidazole results in an increase of the A_{1965} substate population (Figure 4i). Ligand rebinding in this conformation is maximal at ~23 K.

The photoproduct maps show solid as well as dotted contours below 20 K (Figure 4, right column). The solid features indicate a ligand population increase in a particular intermediate site, due to either ligand reorientation or migration between photoproduct sites. The dominant contours are at 2127 cm^{-1} and at either ~35 K (pH 5.5) or 60 K (pH 7, pH 10).

Comparison of the contours in the TDS maps of heme-bound and photolyzed CO indicates that ligands from photoproduct state B_{2128} rebind to A_{1950}, whereas ligands from B_{2134} recombine to A_{1940}. Most of the photolyzed ligands in B_{2118} and B_{2113} do not rebind to the heme iron but reorient at the intermediate docking site, as can be seen from the occurrence of both solid and dotted contours of similar magnitude below 20 K. The presence of TFP leads to recombination from B_{2122} to A_{1972} at ~30 K (Figures 4f and 4h). The analogous photoproduct band of the TBP sample cannot be resolved, most likely due to its low intensity (in comparison to Figure 3).

The mapping between bound-state and photoproduct bands is corroborated by the contour plots of mutant Tyr38Phe (Figures 5a and 5b). As A_{1950} is absent in the protein, A_{1940} and B_{2137} are unambiguously connected. Ligand exchange occurs between B_{2120} and B_{2137} below 25 K; recombination peaks at 50 K. Upon addition of TFP, additional A bands emerge at higher frequencies; the major photoproduct bands are at 2122 and 2128 cm^{-1} (Figures 5c and 5d).

Ligand Recombination from Secondary Docking Sites. The TDS maps obtained after cooling the samples from 160 to 3 K under constant illumination are shown in Figure 6. The contours extend to 130 K as compared to 100 K after brief illumination. At pH 5.5, a second rebinding maximum is well resolved at ~90 K (Figure 6a). It indicates that ligand recombination from a secondary site occurs at essentially the same temperature for all substates. The fraction of ligands trapped at this additional site is ~15% of the total, as seen from the integrated absorbance differences calculated from the DHPCO−TDS maps (Figure 7). The temperatures of maximal recombination from the initial photoproduct site are unchanged with respect to brief illumination. In the presence of TFP, ligand escape to the secondary site is observed for only 9% of all photolyzed ligands (Figures 6e and 6g). A second distinct maximum representing recombination from a secondary site is not resolved at pH 7 and 10 but implicated by the extension of the contours to ~130 K and more clearly visible in Figure 7.

The pH 5 photoproduct map displays ligand rebinding only (Figure 6b). The positive signals assigned to ligand reorientation or migration within the photoproduct states after 1 s of illumination (Figure 4, right column) are essentially absent. Instead, we observe contours between 2130 and 2135 cm^{-1} that extend up to ~120 K. In all other photoproduct maps, the exchange signals have decreased in magnitude but are still present (Figure 6, right column). No pronounced differences are seen in the contour plots at pH 7 and 10.

Absorbance Spectra of a Fluctuating Protein. Between 160 and 295 K, absorbance spectra of 6×His-tagged DHPCO with and without TBP and TFP were collected at different pH values (Supporting Information and Figure 3). At ambient temperature, the CO stretching frequency spectra are essentially identical for any substrate or substrate analogue, which is consistent with a substrate-free distal pocket under all here studied conditions (Supporting Information). The data set for TFP binding consisting of area-normalized absorbance spectra (DHPCO−TFP, pH 5.5, 160−295 K) is plotted in Figure 8. The spectra were fitted to Gaussians to determine the band areas, which were taken to compute fractional populations of DHPCO with TFP (n_{TFP}) and DHPCO without TFP ($n_{w/oTFP}$). They are related to the free energy difference, ΔG

$$\Delta G = -RT \ln K = -RT \ln\left(\frac{n_{TFP}}{n_{w/oTFP}}\right) = \Delta H - T\Delta S \quad (2)$$

with equilibrium coefficient K, temperature T, and gas constant R. The slope in the van't Hoff plot yields an average enthalpy

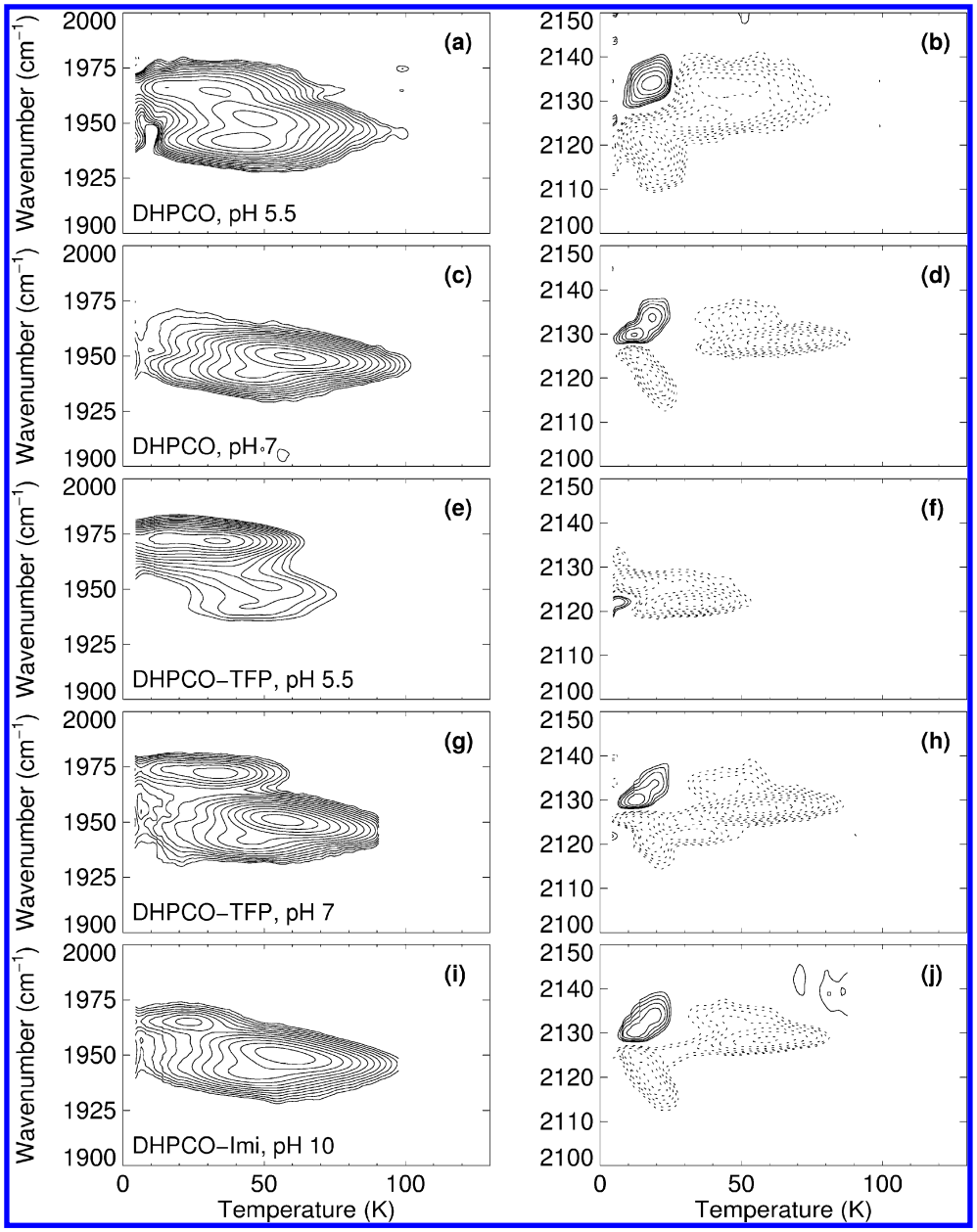

Figure 4. Temperature derivative spectroscopy contour maps of 6×His-tagged DHP taken after 1 s of illumination at 3 K. Absorbance changes of DHPCO at (a, b) pH 5.5, (c, d) pH 7, (e, f) pH 5.5 with TFP, (g, h) pH 7 with TFP, and (i, j) pH 10 are shown for the IR bands of heme-bound CO (left column) and photolyzed CO (right column). Contours are spaced logarithmically; solid (dotted) lines represent increasing (decreasing) absorbance.

difference $\Delta H = -19.8 \pm 0.1$ kJ/mol between the two states (Figure 8, inset), implying that substrate binding is an exothermic process. The solvent in these experiments is a 50% glycerol/buffer solution, and thus the solubility of the substrate is higher than in water. It is remarkable that the substrate is only bound to the CO-ligated form of the protein at low temperature.

Flash Photolysis Experiments. The photoproduct and heme-bound state are separated by an enthalpy barrier against recombination, H. At cryogenic temperatures, each protein molecule is frozen in a slightly different conformation. As a consequence, a distribution of barrier heights $g(H)$ exists within the ensemble of protein molecules that can be determined by flash photolysis experiments carried out over a wide temperature range.[47,48]

The dilute (∼10 μM) DHPCO samples at pH 5 (with and without TFP) and pH 8 (without substrate) were photolyzed with a 6 ns laser flash at temperatures between 20 and 300 K. Samples without substrate were equilibrated with 0.05 bar CO, the one with TFP with 1 bar CO. Ligand recombination was monitored at 436 nm from 30 ns to 1 s (Figure 9). Below the glass transition temperature of the cryosolvent (∼180 K), ligand recombination occurs only from within the protein. The non-exponential geminate process extends over many orders of magnitude in time. Kinetics between 40 and 200 K (Figures 9a−c) were fitted globally with a two-state model that assumes a static distribution of activation enthalpy barriers, $g(H)$, between the bound and the photoproduct states.[47,49] The fraction of heme groups that is still unligated at time t after the flash, $N(t)$, is given by

$$N(t) = \int g(H) \exp[-k(H,T)t]\, dH \qquad (3)$$

The measured absorbance change, $\Delta A(t)$, is taken to be proportional to $N(t)$. For a thermally activated barrier crossing, the dependence of the rebinding rate coefficient $k(H,T)$ on

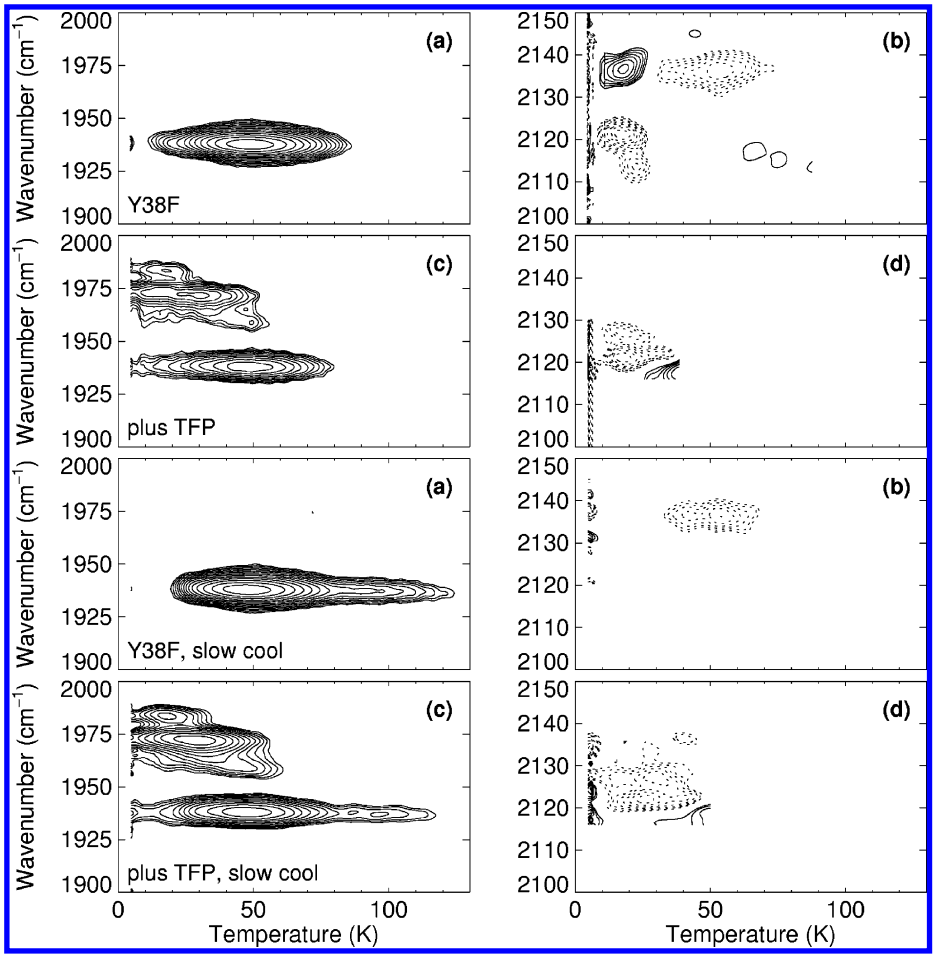

Figure 5. Temperature derivative spectroscopy contour maps of Tyr38PheCO at pH 7.5. (a, b, e, f) 1 s of illumination at 3 K; (c, d, g, h) slow cooling from 160 to 3 K. Absorbance changes are shown for the IR bands of heme-bound CO (left column) and photolyzed CO (right column). Contours are spaced logarithmically; solid (dotted) lines represent increasing (decreasing) absorbance.

temperature T is given by the transition state expression

$$k = A\frac{T}{T_0}\exp\left[-\frac{H}{RT}\right] \tag{4}$$

with preexponential A, reference temperature T_0 set to 100 K, and the universal gas constant R. A Gaussian distribution was chosen as a model function for $g(H)$

$$g(H) = \frac{1}{\sqrt{2\pi\sigma^2}}\exp\left(-\frac{(H-H_p)^2}{2\sigma^2}\right) \tag{5}$$

where H_p is the peak enthalpy and σ is the width of the enthalpy distribution. Nonlinear least-squares fits of eqs 3−5 to the data yielded $A = 10^{9\pm0.5}$ s^{-1}, $\sigma = 3.8 \pm 0.1$ kJ, and $H_p = 9.2 \pm 0.2$ kJ/mol at pH 8 and $A = 10^{8.5\pm0.5}$ s^{-1}, $\sigma = 3.8 \pm 0.2$ kJ, and $H_p = 6.3 \pm 0.1$ kJ/mol at pH 5. In the presence of TFP (pH 5), the enthalpy barrier decreases to $H_p = 3.5 \pm 0.2$ kJ/mol, with $\sigma = 4.5 \pm 0.2$ kJ and $A = 10^{8.4\pm0.5}$ s^{-1}.

The kinetic traces up to 300 K are plotted in Figures 9d−f. A plateau, barely visible at 200 K and more clear at 220 K, indicates that ligand association is not complete within the observation time (here 1 s). At 240 K, a second recombination step becomes evident that speeds up with temperature. It represents CO rebinding from the solvent, which is a bimolecular process that depends on both the concentrations of the protein, [P], and the ligand, [L]. If [L] ≫ [P], then the ligand concentration can be taken as essentially constant during the course of the reaction so that the latter can be described with a pseudo-first-order rate coefficient that depends linearly on the ligand concentration. At 293 K, the bimolecular rate coefficients determined by a fit with a single exponential are 0.98 ± 0.05 μM^{-1} s^{-1} (pH 8, 0.05 bar CO), 1.14 ± 0.05 μM^{-1} s^{-1} (pH 5, 0.05 bar CO), and 1.19 ± 0.03 μM^{-1} s^{-1} (pH 5, TFP, 1 bar CO).

Discussion

Myoglobin was the first protein to have its three-dimensional molecular structure revealed.[50] Whereas early crystallographic studies showed only a single location for the heme-bound CO, the appearance of several CO stretching bands clearly indicated that Mb possesses multiple, markedly different active-site structures.[26,41,51] Detailed FTIR studies of heme-bound and photodissociated CO within the protein as a function of temperature and illumination conditions[28,30,41,43,52] paved the way to X-ray structure determinations of photointermediates by cryogenic trapping[31,32,53,54] and time-resolved diffraction.[33,34,55,56] Only through the combination of spectroscopy and crystallography could a detailed understanding of the role of ligand migration in ligand binding to Mb be achieved.

The structural similarity of DHP and Mb suggests that experiments using CO as a probe should provide specific information on the dynamics of the enzyme active site of DHP. This initial report on the dynamics in DHP demonstrates that all of these experiments are possible on DHP and that they have the potential to address the specific role of substrate binding on the dynamic motions in the distal pocket.

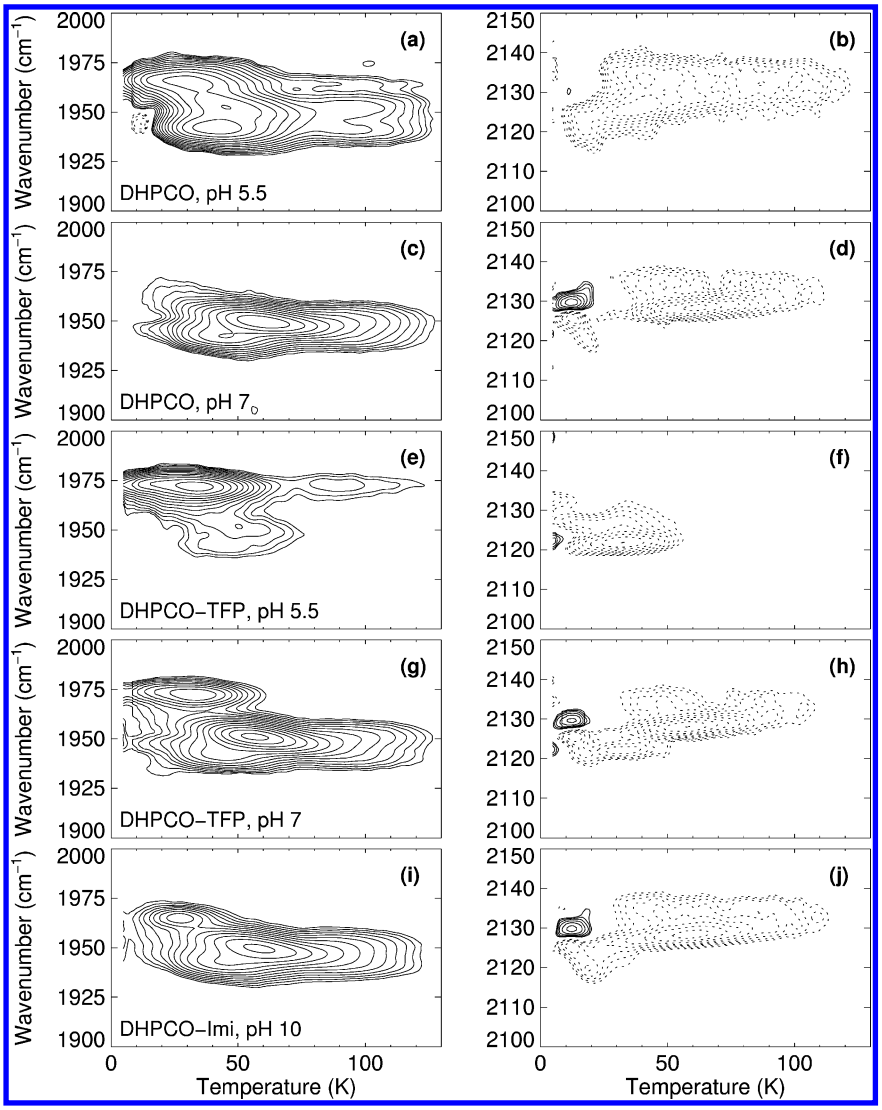

Figure 6. Temperature derivative spectroscopy contour maps of 6×His-tagged DHP computed from spectra taken after slow cooling under illumination from 160 to 3 K. Absorbance changes of DHPCO at (a, b) pH 5.5, (c, d) pH 7, (e, f) pH 5.5 with TFP, (g, h) pH 7 with TFP, and (i, j) pH 10 are shown for the IR bands of heme-bound CO (left column) and photolyzed CO (right column). Contours are spaced logarithmically; solid (dotted) lines represent increasing (decreasing) absorbance.

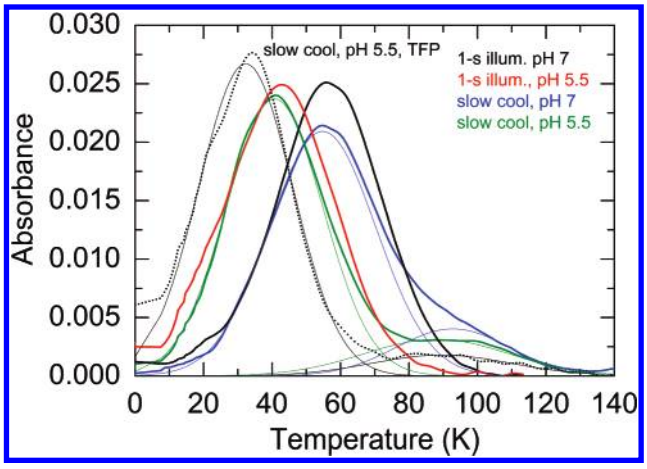

Figure 7. Integrated absorbance differences, $\int \Delta A \, d\nu$, calculated from the TDS experiments on DHPCO after 1 s (black, pH 7; red, pH 5.5) and extended illumination (blue, pH 7; green, pH 5.5; black dotted, pH 5.5, plus TFP). Thick lines depict the data; thin lines represent fits with Gaussian distributions.

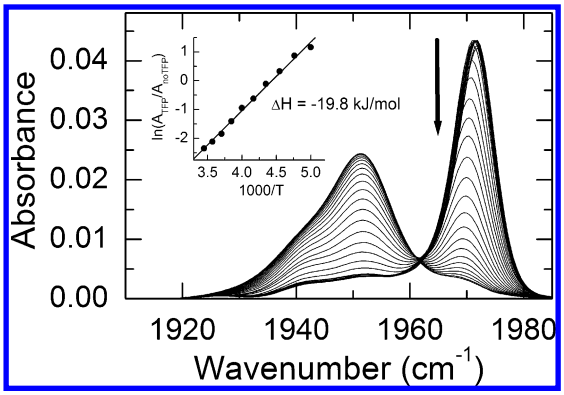

Figure 8. Fourier transform infrared photolysis difference spectra of DHPCO with TFP, pH 5.5, between 160 and 295 K. The arrow indicates increasing temperatures. Inset: van't Hoff plot of the ratio of the fractional populations of DHPCO with TFP (n_{TFP}) and DHPCO without TFP ($n_{w/oTFP}$) as a function of temperature.

The superb properties of the CO molecule as an infrared spectroscopic marker are based on its sensitivity to the surroundings. At the active site of heme proteins, the CO stretching frequency is governed by electrostatic interactions between the CO dipole and the local electric field.[22,23,57,58] The bond between the CO molecule and the heme iron consists of two contributions, a σ-bond due to electron donation from the CO to the

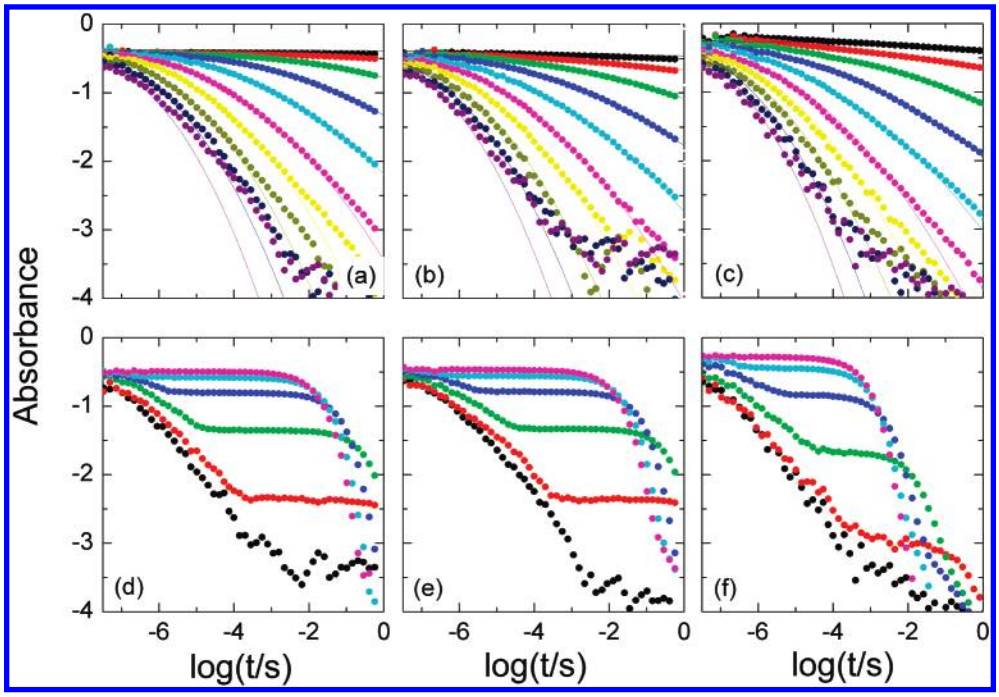

Figure 9. Recombination kinetics of 6×His-tagged DHPCO after 6 ns of illumination, monitored at 436 nm: (a, d) pH 8, 0.05 bar CO; (b, e) pH 5, 0.05 bar CO; (c, f) pH 5, plus TFP, 1 bar CO. (a−c) Kinetic traces at temperatures between 20 and 200 K. (d−f) Kinetic traces at temperatures between 200 and 300 K. Symbols are data; lines represent results from a global fit using eq 3.

iron and a π-back-bonding donation from the iron d_{z^2}-orbital into an antibonding π^*-orbital of the CO. A positive partial charge, e.g., a hydrogen bond X−H···OC, in the vicinity of the ligand oxygen increases the back-bonding contribution, reduces the CO bond strength, and consequently shifts the stretching frequency to lower values. A negative partial charge, e.g., a lone pair directed at the oxygen of CO, has the opposite effect. With the CO molecule as a sensitive gauge, we have investigated the DHP active site to elucidate structurally different and possibly functionally relevant conformations (Figure 1b).

Structural Heterogeneity at the DHP Active Site at Cryogenic Temperatures. The FTIR absorbance spectra of DHPCO show multiple stretching bands of heme-bound CO. The absorbance spectra were determined at different pH values (Figure 2). Moreover, the native substrate TBP and the more soluble TFP as well as imidazole, all of which have pK_a values between 6 and 7, were added as test molecules to understand their influence on the FTIR spectra. It is important to consider that heterogeneity in samples prepared with substrate can arise either from different conformations at the active site or from the coexistence of both substrate-free and substrate-bound forms.

The most pronounced A substate band in DHPCO is at ∼1950 cm^{-1} and thus at a slightly higher frequency than the one of the dominant A_1 band in MbCO (1945 cm^{-1}). The main determinant of the CO stretching frequency in Mb is the electrostatic interaction between the neutral His64 that carries a proton on the N_ϵ and the oxygen of the heme-bound ligand. The 5 cm^{-1} shift in the position of A_{1950} as compared to A_1 in MbCO would suggest a weaker interaction with a positive partial charge. A comparison of the distal pockets reveals that the distance between the N_ϵ−H of the DHP His55 imidazole side chain and the heme iron is larger than that in MbCO (5.48 vs 4.91 Å)[20] (Figure 1b). The distances between the CO oxygen and the N_ϵ−H are estimated as ∼2.3 and ∼3.4 Å in Mb and DHP, respectively. If N_δ were protonated (i.e., in the tautomeric form of a neutral His55), then the free electron pair on N_ϵ would point at the ligand and shift the stretching frequency to markedly higher values, as is observed for Mb mutants Val68Thr[29] and His64Val−Val68Thr.[58] On the basis of these considerations, we conclude that the N_ϵ−H tautomer is present; the observed frequency of 1950 cm^{-1} is consistent with a N_ϵ−H···OC interaction at a slightly longer distance than that in Mb. This interpretation of the electrostatic interactions is based on the X-ray structures of both Mb and DHP, which indicate that the imidazole side chains in DHP and Mb are isomers, rotated around the C_β−C_γ bond (Figure 1b), as these orientations allow for the most efficient hydrogen bonding interactions between the side chains and the neighboring residues.

The position of the band at ∼1940 cm^{-1} indicates that the positive partial charge is closer to the heme-bound ligand. This substate appears similar to A_3 in MbCO, in which the distal histidine side chain is closer to the ligand oxygen.[25] Interestingly, all Tyr38PheCO molecules adopt the A_{1940} conformation, which suggests that an interaction exists between the Tyr38 and His55 side chains. Tyr38 resides in the CD loop at position 4 and studies of CD4 mutants in Mb have shown that the corresponding amino acid Phe46 orients the distal His64 for hydrogen bonding to heme-bound ligands.[38] By the mutation Tyr38Phe, the hydrogen bond interaction between the Tyr38 hydroxyl and the imidazole N_δ (distance 2.67 Å, Figure 1b) is removed. As a result, the imidazole side chain might rotate around the C_β−C_γ bond and adopt the isomer seen in Mb to establish a new hydrogen bond between N_δ and the heme propionate and at the same time position the N_ϵ−H closer to the heme-bound ligand. This suggestion will be further explored by NMR and X-ray crystallography studies of the mutant protein.

On the basis of UV−vis spectroscopy, the pK of the distal His55 is ∼4 (Figure 2c). Therefore, we expect an additional absorbance band at higher frequency to emerge at low pH, because the protonated imidazole side chain should rotate toward the solvent to screen the positive charge,[24,59] and the interaction between His55 and the ligand should no longer exist. This band, A_{1965} (corresponding to A_0 in MbCO, $\nu \approx 1965$ cm^{-1}), indeed appears to account for ∼30% of the total population at pH 5.5 (Table 1).

To further test this band assignment, we have added excess imidazole to 6×His-tagged DHP samples at pH 5.5 and 10. Imidazole enters the distal pocket of DHP, where it replaces the water molecule at the sixth coordination site of the ferric heme iron (Supporting Information). When a CO molecule is bound to the heme iron, the incoming imidazole can mimic a distal histidine and one would expect a gain in the closed conformations. The absorbance spectra in Figure 3 show, however, that the population of the open A_{1965} form increases independent of pH. This finding indicates that in these samples the His55 side chain orients toward the solvent even in the neutral state. A similar, pH-independent increase of the A_0 substate population was observed upon embedding a MbCO sample in trehalose and explained by the decreased water activity that affects the equilibrium between the conformational substates.[60] The same phenomenon might be responsible for the high fraction of the open conformation in the substrate-free crystal grown at high polyethylene glycol and salt concentrations.[20]

After the substrates TBP and TFP were added, a new band appears at ~1972 cm^{-1} in both 6×His-tagged and mutant DHP. The X-ray structure of DHP shows His55 exclusively in the exterior position when substrate is bound.[20,61] As the stretching frequency is identical and independent of the substrate, it is determined by the interaction between the heme-bound ligand and the π-electron system of the aromatic ring system. The shift to higher frequency is similar to a lone pair effect and opposite to the effect of hydrogen bonding. At pH 5.5, ~80% of all DHP molecules bind TFP at cryogenic temperatures, whereas the occupancy with TBP is only ~11%, as seen from the fractional band areas. At pH 7, there is significantly less substrate binding (Figure 3).

The pH dependence can be ascribed to (i) the two different conformations of the His55 imidazole side chain and (ii) the protonation states of the substrates. Protonation of the side chain at low pH favors the open conformation (Figure 1b). Within the same pH region, the substrates are neutral and therefore likely to enter the apolar distal heme pocket. The different degrees of occupancy of TBP and TFP (at 3 K) may have several reasons. The solubility of TFP in water is almost 10 times higher than of that of TBP (70 vs 700 μM). Still, the protein concentration in the present experiments is much higher (~10 mM). Moreover, the TBP molecule is more voluminous than TFP, with empirical covalent radii of fluorine and bromine of 0.71 and 0.114 pm, respectively.[62]

Probing the Active Site at Ambient Temperature. At cryogenic temperatures, both TFP and TBP are accommodated in the DHP distal pocket in amounts sufficient for detection with our spectroscopic methods. For investigation of the enzymatic function, however, it is relevant to study substrate binding near ambient temperature. This turns out to be surprisingly difficult. The van't Hoff plot yields a stabilization of the protein by ~20 kJ/mol upon binding of TFP (Figure 8). Note that in aqueous buffer the solubility of TFP is still lower and the experiment is even more difficult. The apparently very low substrate affinity at ambient temperature seems surprising. But one has to keep in mind that the present studies were performed with a diatomic CO molecule bound to the heme iron, which may prevent the substrate from entering the heme pocket. A recent study has shown that the enzyme is inhibited if H_2O_2 is added prior to TBP.[13] The nature of the inhibition could involve a steric component that prevents the substrate from reaching its binding site once a ligand has bound to the heme iron. The temperature decrease diminishes the mobility of the polypeptide, which may increase the open distal heme pocket volume and thus result in more efficient substrate association.

Ligand Migration and Recombination in DHPCO. In Mb, ligand storage occurs at the heme iron. There are, however, additional transient docking sites in the protein matrix that are essential for ligand association and dissociation. The primary photoproduct site B that mediates ligand binding is in the distal pocket, on top of pyrrole C.[35−37] Moreover, four internal cavities are known that are spacious enough to accommodate Xe atoms. Cavity Xe4 is in the back of the distal pocket (Figure 1a); the Xe1 site is on the proximal side of the heme plane. At these two sites, unbound ligands can reside long enough within the protein matrix to escape by means of large-scale protein fluctuations instead of rebinding.[28] Xe2 and Xe3 do not serve as docking sites. They are most likely part of the channel that transiently connects the distal and proximal sites.[63,64]

The TDS experiments presented here provide information on ligand migration to transient docking sites in DHP. After 1 s of illumination at 3 K, ligand recombination in each conformational substate occurs from a single transient docking site, which we will denote as the primary docking site B (Figure 6). The dominant photoproduct band in 6×His-tagged DHPCO (pH 7) is at ~2127 cm^{-1} (Figure 3). On the basis of the TDS data, this photoproduct band corresponds to photolyzed CO ligands recombining in molecules of the A_{1950} conformation. The photoproduct band corresponding to the opposite orientation of the CO at the same site is not observed, possibly because the Stark splitting is too small.[65] The weak signals at 2127 and 2128 cm^{-1} and 12 K with opposite signs that are visible in the TDS maps at pH 7 and 10 (Figures 6d and 6j) might be caused by ligand reorientation at site B. The TDS maps of Tyr38Phe show only photoproduct bands associated with A_{1940} and thus allow a definitive assignment (Figure 7). Positive and negative contours at 2123 and 2137 cm^{-1} peaking at ~20 K provide evidence of ligand rotation at site B in A_{1940} molecules.

The presence of TBP and especially TFP results in a single, new photoproduct band at 2122 cm^{-1} (Figure 3), which confirms an interaction between substrate and photolyzed ligand. Hence, site B is close to the substrate-binding site. The frequency shift may be due solely to electrostatic interactions between the CO and the substrate. However, it is also possible that the substrate occupies or occludes the regular primary photoproduct site and forces the CO into a different position or orientation. The X-ray structure shows that a location analogous to the primary docking site B of Mb is only accessible to the CO if no substrate is present.[20]

In A_{1940} and A_{1950}, ligand rebinding from the primary docking site B occurs at 50−60 K (pH 7) and 30−40 K (pH 5.5) (Figure 4). The difference in temperature reflects higher barriers at pH 7, which is in agreement with the flash photolysis experiments with monitoring in the visible (Figure 9). The Gaussian enthalpy barrier distributions peaked at 9.2 and 6.2 kJ/mol at pH 7 and pH 5.5, respectively. In these measurements, we are only sensitive to the overall ligation state at the heme iron but cannot resolve the contributions from the different A substates. Consequently, we determine the average enthalpy barrier distribution $g(H)$ of all proteins in the ensemble.

The distribution of enthalpy barriers within each conformational substate, $g(H)$, arises from structural heterogeneity of the frozen sample. It also leads to inhomogeneous broadening of the spectral lines. As both spectroscopic and functional parameters depend on structural properties, they are often correlated. For example, the position of an absorbance band and the barrier height might be determined by the same structural parameter.

As a consequence, rebinding is accompanied by a characteristic spectral shift denoted as "kinetic hole burning" (KHB).[49,66−68] The A state maps (Figure 4, left column) indeed show such a pronounced shift toward lower wavenumber with increasing temperature. Recombination depletes the photolysis-induced absorbance difference band from the high-wavenumber edge. Hence, one can conclude that the ligands encountering smaller enthalpy barriers give rise to a high-frequency band when bound at the heme iron. The line shift is identical at pH 5.5 and 7. The lower average rebinding temperature at low pH implies that a larger fraction of CO ligands rebinds over lower barriers and thus gives rise to homogeneous components with higher frequencies. In fact, the stretching frequencies of A_{1940} and A_{1950} at 3 K are higher at pH 5.5 than those at pH 7 (Table 1).

It is likely that KHB in DHP is due to a distribution of His55 side chain positions. Within one A substate, the side chain can adopt many slightly different orientations. If it is oriented more toward the solvent, then the stretching frequency shifts to higher wavenumbers, and the steric hindrance against rebinding is reduced. Further experiments on select mutant samples are necessary to confirm this suggestion.

In the open A_{1965} conformation (without substrate), recombination occurs at significantly lower temperatures as compared to A_{1940} and A_{1950}. This difference has also been monitored for rebinding in the A_0 substate of MbCO.[28,43,59,69] Structurally, the lower barrier may arise from the fact that the heme iron is more readily accessible, as the steric hindrance by the imidazole side chain is absent. Moreover, the hydrogen bonding between the CO molecule at the primary docking site and the distal histidine may increase the barrier to rebinding in the closed conformation.[65] Low rebinding temperatures are also found in the presence of substrate. The global fit of the kinetic traces in Figure 9c yields an average enthalpy barrier of 3.5 kJ/mol that is markedly lower than that found in the sample without TFP. With the imidazole side chain in the open conformation, the voluminous substrate occupies a large fraction of the distal pocket. Therefore, it might trap the photolyzed CO ligand close to the active site and hinder access to the primary docking site B.

On the basis of the similarity of the three-dimensional folds of DHP and Mb (compare Figure 1), it seems likely that DHP also possesses internal cavities that might be functionally important for ligand storage. The TDS maps after extended illumination reveal, however, that only about 10% of all photolyzed ligands escape to a secondary docking site from where they rebind at ∼80 K and thus at a temperature similar to that in Mb.[28,41,43] A closer look at the X-ray structure shows that residues Ala17, Ile20, Phe21, Thr56, Val59, Phe60, Met63, Leu100, and Leu104 enclose an open volume similar to Xe4 in Mb. With the Phe21 side chain rotated by ∼90° (Figure 1), this Xe4 analogue becomes part of the enlarged distal pocket. The Xe1 analogue is at least partially occluded by residue Phe97. Moreover, the Phe101 and Phe123 side chains are pointed into the Xe2 and Xe3 cavities and thus reduce their volumes. With only the Xe4 analogue accessible to photolyzed ligands, secondary sites do not appear to be essential for the protein to perform its function (Figure 7). Hence, the protein seems designed for peroxidase activity but not for oxygen storage.

Oxygen Storage versus Peroxidase Activity. Peroxidases carry out substrate oxidation using H_2O_2. The reaction involves cleavage of the hydrogen peroxide O−O bond via a so-called push−pull mechanism.[16] The reactivity of the heme is thought to be governed by several factors: (i) axial ligands, (ii) distal residues, and (iii) solvent accessibility of the metal center.

In DHP, the heme is anchored within the polypeptide moiety via the proximal histidine. Strong hydrogen bonding interactions between the N_δ−H of the proximal histidine and an aspartate is hypothesized to stabilize higher oxidation states of the iron in HRP and cytochrome c peroxidase.[70−73] As a consequence, the axial ligand gains imidazolate character, which leads to a stronger interaction with the heme iron. The X-ray structure of DHP shows that the imidazole side chain is rotated by ∼60° as compared to Mb and its hydrogen atom forms a hydrogen bond with the backbone carbonyl oxygen of Leu83 (length 2.7 Å) that is most likely stronger than that in Mb.[20] Resonance Raman data indeed indicate that the Fe−His stretching frequency of DHP, ν(Fe−His) ≈ 233 cm^{-1}, is intermediate between the values of sperm whale Mb (∼220 cm^{-1}) and HRP (∼243 cm^{-1}).[1] Hence, the electron push is more intense than that in globins but not as strong as that in typical peroxidases.[74] Computational studies indicate that the protonation state of the proximal histidine does not significantly alter the electronic structure of compound I.[75] Therefore, the role of the proximal ligand may be less important than previously assumed.

The DHP distal heme pocket is more spacious than that of Mb. The phenyl side chain of amino acid Phe21, which forms the physical separation between the heme pocket and the Xe4 site in Mb, is rotated by ∼90° with respect to the orientation in Mb so as to connect both sites (Figure 1b), thereby forming an open volume that suffices to accommodate the bulky aromatic substrate. The orientation of the Phe21 aromatic ring seems predisposed for π-stacking with the phenolic substrate. This interaction could be important for the correct positioning of the substrate for the subsequent oxidation reaction. Because of the bulky substrate, all enzymatic activity most likely takes place in the distal pocket; substrate migration within the protein is highly unlikely.

The distal histidine in peroxidases is thought to serve as an acid−base catalyst, whereas a distal arginine promotes polarization of the hydrogen peroxide O−O bond[1,6] For cytochrome c peroxidase[76,77] and HRP,[78−80] the enzymatic activity was not as significantly affected by the mutation of the arginine as by replacing the histidine. Dehaloperoxidase and myoglobin both lack the arginine but contain the distal histidine. However, their active sites differ in the distances between the imidazole side chain and the ferric heme iron (Figure 1b). In Mb, His64 is at a position designed to stabilize a heme-bound diatomic ligand via hydrogen bonding interactions. The peroxidase activity of Mb can be enhanced by repositioning the distal histidine.[4−6] Myoglobin double mutant Phe43His−His64Leu has an ∼11-fold higher activity; its His43 is 5.4 Å away from the ferric iron and thus at a distance similar to that in DHP (∼5.5 Å). In contrast, the activity is completely lost in the Mb mutant Leu29His−His64Leu, where the histidine−iron distance is 6.6 Å.

It is remarkable that DHP has ∼13 times enhanced peroxidase activity as compared to Mb,[13] although the X-ray structure of DHP shows its distal histidine in a solvent-exposed conformation when the substrate is bound[20] so that it cannot activate the incoming cosubstrate. However, His55 allows easy access of the bulky substrate into the distal heme pocket in this conformation. Our observation that both TFP and TBP bind to CO-ligated DHP only to a significant extent at low temperature implies that the substrate enters the protein before the cosubstrate H_2O_2 binds. Then, once substrate and cosubstrate are bound, the His55 imidazole is likely to fluctuate into the closed conformation in which it can readily activate the cosubstrate.

Conclusions

We have experimentally characterized thermodynamic and spectroscopic effects of substrate binding in DHP from *Amphitrite ornata* using CO as a probe molecule of the active site. Typical CO stretching frequencies for a closed (1950 cm^{-1}) and an open (1965 cm^{-1}) conformation of the distal His55 are observed that have a strong analogy with the closed and open conformations of the distal His64 in Mb. Substrate binding, which occurs preferentially at low temperature and low pH, shifts the stretching frequency of heme-bound CO to 1972 cm^{-1}. This spectral shift is consistent with a nonbonding, electrostatic interaction between the phenol ring of the substrate and the CO.

Additional similarities with Mb are apparent, including the presence of a nearby docking site and at least one further site in the protein where photolyzed CO molecules can reside. Moreover, a bound substrate traps the photolyzed ligand closer to the binding site and thus lowers the energy barriers for geminate CO recombination as seen from the flash photolysis experiments.

However, the experiments also raise an interesting question and a hypothesis for further investigation. Why do we observe a steric interference between the substrate and the CO molecule at pH 5−7 and ambient temperature, which are precisely the conditions where DHP has the greatest enzymatic activity? Dehaloperoxidase is both a globin and an enzyme. In its globin function, DHP binds oxygen reversibly. Substrate binding itself may trigger the peroxidase activity. If this is the case, then the investigation of the interaction between probe molecules such as CO and substrate will provide key information on the function switch in the enzyme.

Acknowledgment. G.U.N. acknowledges financial support by the Deutsche Forschungsgemeinschaft (Grant No. Ni291/3) and the Fonds der Chemischen Industrie. S.F. acknowledges financial support by the National Science Foundation (Grant No. MCB-9874895).

Supporting Information Available: UV−visible spectra of ferric DHP upon addition of imidazole and room temperature FTIR spectra of all DHPCO samples presented in Figure 3. This material is available free of charge via the Internet at http://pubs.acs.org.

References and Notes

(1) Franzen, S.; Roach, M. P.; Chen, Y.-P.; Dyer, R. B.; Woodruff, W. H.; Dawson, J. H. The unusual reactivities of *Amphitrite ornata* dehaloperoxidase and *Notomastus lobatus* chloroperoxidase do not arise from a histidine imidazolate proximal heme iron ligand. *J. Am. Chem. Soc.* **1998**, *120*, 4658−4661.

(2) Antonini, E.; Brunori, M. *Hemoglobin and Myoglobin in Their Reactions with Ligands*; North-Holland: Amsterdam, 1971.

(3) Flögel, U.; Merx, M. W.; Godecke, A.; Decking, U. K.; Schrader, J. Myoglobin: A scavenger of bioactive NO. *Proc. Natl. Acad. Sci. U.S.A.* **2001**, *98*, 735−740.

(4) Matsui, T.; Ozaki, S.; Liong, E.; Phillips, G. N., Jr.; Watanabe, Y. Effects of the location of distal histidine in the reaction of myoglobin with hydrogen peroxide. *J. Biol. Chem.* **1999**, *274*, 2838−2844.

(5) Ozaki, S.; Roach, M. P.; Matsui, T.; Watanabe, Y. Investigations of the roles of the distal heme environment and the proximal heme iron ligand in peroxide activation by heme enzymes via molecular engineering of myoglobin. *Acc. Chem. Res.* **2001**, *34*, 818−825.

(6) Roach, M. P.; Puspita, W. J.; Watanabe, Y. Proximal ligand control of heme iron coordination structure and reactivity with hydrogen peroxide: Investigations of the myoglobin cavity mutant H93G with unnatural oxygen donor proximal ligands. *J. Inorg. Biochem.* **2000**, *81*, 173−182.

(7) Egawa, T.; Yoshioka, S.; Takahashi, S.; Hori, H.; Nagano, S.; Shimada, H.; Ishimori, K.; Morishima, I.; Suematsu, M.; Ishimura, Y. Kinetic and spectroscopic characterization of a hydroperoxy compound in the reaction of native myoglobin with hydrogen peroxide. *J. Biol. Chem.* **2003**, *278*, 41597−41606.

(8) Svistunenko, D. A. Reaction of haem containing proteins and enzymes with hydroperoxides: The radical view. *Biochim. Biophys. Acta* **2005**, *1707*, 127−155.

(9) Chen, Y. P.; Woodin, S. A.; Lincoln, D. E.; Lovell, C. R. An unusual dehalogenating peroxidase from the marine terebellid polychaete *Amphitrite ornata*. *J. Biol. Chem.* **1996**, *271*, 4609−4612.

(10) Roach, M. P.; Chen, Y. P.; Woodin, S. A.; Lincoln, D. E.; Lovell, C. R.; Dawson, J. H. *Notomastus lobatus* chloroperoxidase and *Amphitrite ornata* dehaloperoxidase both contain histidine as their proximal heme iron ligand. *Biochemistry* **1997**, *36*, 2197−2202.

(11) Chen, Y. P.; Lincoln, D. E.; Woodin, S. A.; Lovell, C. R. Purification and properties of a unique flavin-containing chloroperoxidase from the capitellid polychaete *Notomastus lobatus*. *J. Biol. Chem.* **1991**, *266*, 23909−23915.

(12) Woodin, S. A.; Marinelli, R. L.; Lincoln, D. E. *J. Chem. Ecol.* **1993**, *19*, 517−530.

(13) Belyea, J.; Godek, M.; Davis, M. F.; Gilvey, L. B.; Sit, T. L.; Lommel, S. A.; Franzen, S. Enzyme function of the globin dehaloperoxidase from *Amphitrite ornata* is activated by substrate binding. *Biochemistry* **2005**, *44*, 15637−15644.

(14) Berglund, G. I.; Carlsson, G. H.; Smith, A. T.; Szoke, H.; Henriksen, A.; Hajdu, J. The catalytic pathway of horseradish peroxidase at high resolution. *Nature* **2002**, *417*, 463−468.

(15) Ward, G.; Hadar, Y.; Bilkis, I.; Dosoretz, C. G. Mechanistic features of lignin peroxidase-catalyzed oxidation of substituted phenols and 1,2-dimethoxyarenes. *J. Biol. Chem.* **2003**, *278*, 39726−39734.

(16) Poulos, T. L.; Kraut, J. The stereochemistry of peroxidase catalysis. *J. Biol. Chem.* **1980**, *255*, 8199−8205.

(17) Henriksen, A.; Schuller, D. J.; Meno, K.; Welinder, K. G.; Smith, A. T.; Gajhede, M. Structural interactions between horseradish peroxidase C and the substrate benzhydroxamic acid determined by X-ray crystallography. *Biochemistry* **1998**, *37*, 8054−8060.

(18) Henriksen, A.; Smith, A. T.; Gajhede, M. The structures of the horseradish peroxidase C−ferulic acid complex and the ternary complex with cyanide suggest how peroxidases oxidize small phenolic substrates. *J. Biol. Chem.* **1999**, *274*, 35005−35011.

(19) Poulos, T. L. The role of the proximal ligand in heme enzymes. *J. Biol. Inorg. Chem.* **1996**, *1*, 356−359.

(20) LaCount, M. W.; Zhang, E.; Chen, Y. P.; Han, K.; Whitton, M. M.; Lincoln, D. E.; Woodin, S. A.; Lebioda, L. The crystal structure and amino acid sequence of dehaloperoxidase from *Amphitrite ornata* indicate common ancestry with globins. *J. Biol. Chem.* **2000**, *275*, 18712−18716.

(21) Ator, M. A.; Ortiz de Montellano, P. R. Protein control of prosthetic heme reactivity. Reaction of substrates with the heme edge of horseradish peroxidase. *J. Biol. Chem.* **1987**, *262*, 1542−1551.

(22) Li, T.; Quillin, M. L.; Phillips, G. N., Jr.; Olson, J. S. Structural determinants of the stretching frequency of CO bound to myoglobin. *Biochemistry* **1994**, *33*, 1433−1446.

(23) Ray, G. B.; Li, X.-Y.; Ibers, J. A.; Sessler, J. L.; Spiro, G. S. How far can proteins bend the FeCO unit? Distal polar and steric effects in heme proteins and models. *J. Am. Chem. Soc.* **1994**, *116*, 162−176.

(24) Yang, F.; Phillips, G. N., Jr. Crystal structures of CO-, deoxy-, and met-myoglobins at various pH values. *J. Mol. Biol.* **1996**, *256*, 762−774.

(25) Vojtechovsky, J.; Chu, K.; Berendzen, J.; Sweet, R. M.; Schlichting, I. Crystal structures of myoglobin−ligand complexes at near-atomic resolution. *Biophys. J.* **1999**, *77*, 2153−2174.

(26) Alben, J. O.; Beece, D.; Bowne, S. F.; Doster, W.; Eisenstein, L.; Frauenfelder, H.; Good, D.; McDonald, J. D.; Marden, M. C.; Moh, P. P.; Reinisch, L.; Reynolds, A. H.; Shyamsunder, E.; Yue, K. T. Infrared spectroscopy of photodissociated carboxymyoglobin at low temperatures. *Proc. Natl. Acad. Sci. U.S.A.* **1982**, *79*, 3744−3748.

(27) Nienhaus, K.; Kriegl, J. M.; Nienhaus, G. U. Structural Dynamics in the active site of murine neuroglobin and its effects on ligand binding. *J. Biol. Chem.* **2004**, *279*, 22944−22952.

(28) Nienhaus, K.; Deng, P.; Kriegl, J. M.; Nienhaus, G. U. Structural dynamics of myoglobin: The effect of internal cavities on ligand migration and binding. *Biochemistry* **2003**, *42*, 9647−9658.

(29) Nienhaus, K.; Deng, P.; Olson, J. S.; Warren, J. J.; Nienhaus, G. U. Structural dynamics of myoglobin: Ligand migration and binding in valine 68 mutants. *J. Biol. Chem.* **2003**, *278*, 42532−42544.

(30) Lamb, D. C.; Nienhaus, K.; Arcovito, A.; Draghi, F.; Miele, A. E.; Brunori, M.; Nienhaus, G. U. Structural dynamics of myoglobin: Ligand migration among protein cavities studied by Fourier transform infrared/temperature derivative spectroscopy. *J. Biol. Chem.* **2002**, *277*, 11636−11644.

(31) Ostermann, A.; Waschipky, R.; Parak, F. G.; Nienhaus, G. U. Ligand binding and conformational motions in myoglobin. *Nature* **2000**, *404*, 205−208.

(32) Chu, K.; Vojtechovsky, J.; McMahon, B. H.; Sweet, R. M.; Berendzen, J.; Schlichting, I. Structure of a ligand-binding intermediate in wild-type carbonmonoxy myoglobin. *Nature* **2000**, *403*, 921−923.

(33) Bourgeois, D.; Vallone, B.; Schotte, F.; Arcovito, A.; Miele, A. E.; Sciara, G.; Wulff, M.; Anfinrud, P.; Brunori, M. Complex landscape of protein structural dynamics unveiled by nanosecond Laue crystallography. *Proc. Natl. Acad. Sci. U.S.A.* **2003**, *100*, 8704−8709.

(34) Schotte, F.; Lim, M.; Jackson, T. A.; Smirnov, A. V.; Soman, J.; Olson, J. S.; Phillips, G. N., Jr.; Wulff, M.; Anfinrud, P. A. Watching a protein as it functions with 150-ps time-resolved X-ray crystallography. *Science* **2003**, *300*, 1944−1947.

(35) Schlichting, I.; Berendzen, J.; Phillips, G. N., Jr.; Sweet, R. M. Crystal structure of photolysed carbonmonoxy-myoglobin. *Nature* **1994**, *371*, 808−812.

(36) Teng, T. Y.; Srajer, V.; Moffat, K. Photolysis-induced structural changes in single crystals of carbonmonoxy myoglobin at 40 K. *Nat. Struct. Biol.* **1994**, *1*, 701−705.

(37) Hartmann, H.; Zinser, S.; Komninos, P.; Schneider, R. T.; Nienhaus, G. U.; Parak, F. X-ray structure determination of a metastable state of carbonmonoxy myoglobin after photodissociation. *Proc. Natl. Acad. Sci. U.S.A.* **1996**, *93*, 7013−7016.

(38) Lai, H. H.; Li, T.; Lyons, D. S.; Phillips, G. N., Jr.; Olson, J. S.; Gibson, Q. H. Phe-46(CD4) orients the distal histidine for hydrogen bonding to bound ligands in sperm whale myoglobin. *Proteins* **1995**, *22*, 322−339.

(39) Belyea, J.; Chaudhary, C.; Sit, T.; Lommel, S.; Franzen, S. Proximal cavity, distal histidine and substrate hydrogen-bonding mutations modulate the activity of the globin dehaloperoxidase from *Amphitrite ornata*. *Biochemistry*, submitted for publication.

(40) Berendzen, J.; Braunstein, D. Temperature-derivative spectroscopy: A tool for protein dynamics. *Proc. Natl. Acad. Sci. U.S.A.* **1990**, *87*, 1−5.

(41) Nienhaus, G. U.; Mourant, J. R.; Chu, K.; Frauenfelder, H. Ligand binding to heme proteins: The effect of light on ligand binding in myoglobin. *Biochemistry* **1994**, *33*, 13413−13430.

(42) Mourant, J. R.; Braunstein, D. P.; Chu, K.; Frauenfelder, H.; Nienhaus, G. U.; Ormos, P.; Young, R. D. Ligand binding to heme proteins: II. Transitions in the heme pocket of myoglobin. *Biophys. J.* **1993**, *65*, 1496−1507.

(43) Nienhaus, G. U.; Chu, K.; Jesse, K. Structural heterogeneity and ligand binding in carbonmonoxy myoglobin crystals at cryogenic temperatures. *Biochemistry* **1998**, *37*, 6819−6823.

(44) Kriegl, J. M.; Nienhaus, K.; Deng, P.; Fuchs, J.; Nienhaus, G. U. Ligand dynamics in a protein internal cavity. *Proc. Natl. Acad. Sci. U.S.A.* **2003**, *100*, 7069−7074.

(45) Lehle, H.; M.; K. J.; Nienhaus, K.; Deng, P.; Fengler, S.; Nienhaus, G. U. Probing electric fields in protein cavities by using the vibrational Stark effect of carbon monoxide. *Biophys. J.* **2005**, *88*, 1978−1990.

(46) Smulevich, G. Understanding heme cavity structure of peroxidases: Comparison of electronic absorption and resonance Raman spectra with crystallographic results. *Biospectroscopy* **1998**, *4*, S3−S17.

(47) Austin, R. H.; Beeson, K. W.; Eisenstein, L.; Frauenfelder, H.; Gunsalus, I. C. Dynamics of ligand binding to myoglobin. *Biochemistry* **1975**, *14*, 5355−5373.

(48) Nienhaus, G. U.; Young, R. D. Protein Dynamics. In *Encyclopedia of Applied Physics*; Trigg, G. L., Ed.; VCH Publishers: New York, 1996; Vol. 15, pp 163−184.

(49) Steinbach, P. J.; Ansari, A.; Berendzen, J.; Braunstein, D.; Chu, K.; Cowen, B. R.; Ehrenstein, D.; Frauenfelder, H.; Johnson, J. B.; Lamb, D. C.; Luck, S.; Mourant, J. R.; Nienhaus, G. U.; Ormos, P.; Philipp, R.; Xie, A.; Young, R. D. Ligand binding to heme proteins: Connection between dynamics and function. *Biochemistry* **1991**, *30*, 3988−4001.

(50) Kendrew, J. C.; Bodo, G.; Dintzis, H. M.; Parrish, R. G.; Wyckoff, H.; Phillips, D. C. A three-dimensional model of the myoglobin molecule obtained by X-ray analysis. *Nature* **1991**, *181*, 662−666.

(51) Caughey, W. S.; Shimada, H.; Choc, M. G.; Tucker, M. P. Dynamic protein structures: Infrared evidence for four discrete rapidly interconverting conformers at the carbon monoxide binding site of bovine heart myoglobin. *Proc. Natl. Acad. Sci. U.S.A.* **1981**, *78*, 2903−2907.

(52) Nienhaus, G. U.; Mourant, J. R.; Frauenfelder, H. Spectroscopic evidence for conformational relaxation in myoglobin. *Proc. Natl. Acad. Sci. U.S.A.* **1992**, *89*, 2902−2906.

(53) Brunori, M.; Vallone, B.; Cutruzzola, F.; Travaglini-Allocatelli, C.; Berendzen, J.; Chu, K.; Sweet, R. M.; Schlichting, I. The role of cavities in protein dynamics: Crystal structure of a photolytic intermediate of a mutant myoglobin. *Proc. Natl. Acad. Sci. U.S.A.* **2000**, *97*, 2058−2063.

(54) Nienhaus, K.; Ostermann, A.; Nienhaus, G. U.; Parak, F. G.; Schmidt, M. Ligand migration and protein fluctuations in myoglobin mutant L29W. *Biochemistry* **2005**, *44*, 5095−105.

(55) Srajer, V.; Ren, Z.; Teng, T. Y.; Schmidt, M.; Ursby, T.; Bourgeois, D.; Pradervand, C.; Schildkamp, W.; Wulff, M.; Moffat, K. Protein conformational relaxation and ligand migration in myoglobin: A nanosecond to millisecond molecular movie from time-resolved Laue X-ray diffraction. *Biochemistry* **2001**, *40*, 13802−13815.

(56) Hummer, G.; Schotte, F.; Anfinrud, P. A. Unveiling functional protein motions with picosecond X-ray crystallography and molecular dynamics simulations. *Proc. Natl. Acad. Sci. U.S.A.* **2004**, *101*, 15330−15334.

(57) Franzen, S. An electrostatic model for the frequency shifts in the carbonmonoxy stretching band of myoglobin: Correlation of hydrogen bonding and the Stark tuning rate. *J. Am. Chem. Soc.* **2002**, *124*, 13271−13281.

(58) Phillips, G. N., Jr.; Teodoro, M. L.; Li, T.; Smith, B.; Olson, J. S. Bound CO is a molecular probe of electrostatic potential in the distal pocket of myoglobin. *J. Phys. Chem. B* **1999**, *103*, 8817−8829.

(59) Müller, J. D.; McMahon, B. H.; Chien, E. Y.; Sligar, S. G.; Nienhaus, G. U. Connection between the taxonomic substates and protonation of histidines 64 and 97 in carbonmonoxy myoglobin. *Biophys. J.* **1999**, *77*, 1036−1051.

(60) Librizzi, F.; Viappiani, C.; Abbruzzetti, S.; Cordone, L. Residual water modulates the dynamics of the protein and of the external matrix in "trehalose coated" MbCO: An infrared and flash-photolysis study. *J. Chem. Phys.* **2002**, *116*, 1193−1200.

(61) Lebioda, L.; LaCount, M. W.; Zhang, E.; Chen, Y. P.; Han, K.; Whitton, M. M.; Lincoln, D. E.; Woodin, S. A. An enzymatic globin from a marine worm. *Nature* **1999**, *401*, 445.

(62) WebElements Periodic Table. http://www.webelements.com.

(63) Bossa, C.; Amadei, A.; Daidone, I.; Anselmi, M.; Vallone, B.; Brunori, M.; Di Nola, A. Molecular dynamics simulation of sperm whale myoglobin: Effects of mutations and trapped CO on the structure and cavities dynamics. *Biophys. J.* **2005**, *89*, 465−474.

(64) Bossa, C.; Anselmi, M.; Roccatano, D.; Amadei, A.; Vallone, B.; Brunori, M.; Di Nola, A. Extended molecular dynamics simulation of the carbon monoxide migration in sperm whale myoglobin. *Biophys.* **2004**. *J. 86*, 3855−3862.

(65) Nienhaus, K.; Olson, J. S.; Franzen, S.; Nienhaus, G. U. The origin of Stark splitting in the initial photoproduct state of MbCO. *J. Am. Chem. Soc.* **2005**, *127*, 40−41.

(66) Campbell, B. F.; Chance, M. R.; Friedman, J. M. Linkage of functional and structural heterogeneity in proteins: Dynamic hole burning in carboxymyoglobin. *Science* **1987**, *238*, 373−6.

(67) Ormos, P.; Ansari, A.; Braunstein, D.; Cowen, B. R.; Frauenfelder, H.; Hong, M. K.; Iben, I. E.; Sauke, T. B.; Steinbach, P. J.; Young, R. D. Inhomogeneous broadening in spectral bands of carbonmonoxymyoglobin. The connection between spectral and functional heterogeneity. *Biophys. J.* **1990**, *57*, 191−199.

(68) Ormos, P.; Szaraz, S.; Cupane, A.; Nienhaus, G. U. Structural factors controlling ligand binding to myoglobin: A kinetic hole-burning study. *Proc. Natl. Acad. Sci. U.S.A.* **1998**, *95*, 6762−6767.

(69) Young, R. D.; Bowne, S. F. Conformational substates and barrier height distributions in ligand binding to heme proteins. *J. Chem. Phys.* **1984**, *81*, 3730−3737.

(70) Hirst, J.; Wilcox, S. K.; Ai, J.; Moenne-Loccoz, P.; Loehr, T. M.; Goodin, D. B. Replacement of the axial histidine ligand with imidazole in cytochrome c peroxidase. 2. Effects on heme coordination and function. *Biochemistry* **2001**, *40*, 1274−1283.

(71) Hirst, J.; Wilcox, S. K.; Williams, P. A.; Blankenship, J.; McRee, D. E.; Goodin, D. B. Replacement of the axial histidine ligand with imidazole in cytochrome c peroxidase. 1. Effects on structure. *Biochemistry* **2001**, *40*, 1265−1273.

(72) Spiro, T. G.; Smulevich, G.; Su, C. Probing protein structure and dynamics with resonance Raman spectroscopy: Cytochrome c peroxidase and hemoglobin. *Biochemistry* **1990**, *29*, 4497−4508.

(73) Goodin, D. B.; McRee, D. E. The Asp-His-Fe triad of cytochrome c peroxidase controls the reduction potential, electronic structure, and coupling of the tryptophan free radical to the heme. *Biochemistry* **1993**, *32*, 3313−3324.

(74) Franzen, S. Effect of a charge relay on the vibrational frequencies of carbonmonoxy iron porphine adducts: The coupling of changes in axial ligand bond strength and porphine core size. *J. Am. Chem. Soc.* **2001**, *123*, 12578−12589.

(75) Harris, D. L.; Loew, G. H. Proximal ligand effetcs on electronic structure and spectra of compound I of peroxidases. *J. Porphyrins Phthalocyanines* **2001**, *3*, 334−344.

(76) Erman, J. E.; Vitello, L. B.; Miller, M. A.; Shaw, A.; Brown, K. A.; Kraut, J. Histidine 52 is a critical residue for rapid formation of cytochrome c peroxidase compound I. *Biochemistry* **1993**, *32*, 9798−9806.

(77) Vitello, L. B.; Erman, J. E.; Miller, M. A.; Wang, J.; Kraut, J. Effect of arginine-48 replacement on the reaction between cytochrome c peroxidase and hydrogen peroxide. *Biochemistry* **1993**, *32*, 9807−9818.

(78) Tanaka, M.; Ishimori, K.; Mukai, M.; Kitagawa, T.; Morishima, I. Catalytic activities and structural properties of horseradish peroxidase distal His42 → Glu or Gln mutant. *Biochemistry* **1997**, *36*, 9889−9898.

(79) Savenkova, M. I.; Newmyer, S. L.; Montellano, P. R. Rescue of His-42 → Ala horseradish peroxidase by a Phe-41 → His mutation. Engineering of a surrogate catalytic histidine. *J. Biol. Chem.* **1996**, *271*, 24598−24603.

(80) Newmyer, S. L.; de Montellano, P. R. Rescue of the catalytic activity of an H42A mutant of horseradish peroxidase by exogenous imidazoles. *J. Biol. Chem.* **1996**, *271*, 14891−14896.